Chapter

Overview of Hydrological Dynamics and Geomorphological Aspects of the Amazon Region Rivers to Characterize Fluvial Sensitivity to Oil Spills

Patricia Mamede da Silva, Fernando Pellon de Miranda, Carlos Henrique Beisl, Luiz Landau and Alexandre Gonçalves Evsukoff

Abstract

This chapter presents a collection of studies performed in the Amazon region that includes thematic products portraying its fluvial sensitivity to oil spills. The research addresses the intense Amazonian seasonal dynamics, as well as the environmental peculiarities of this singular ecosystem. Periodic changes caused by natural phenomena have a significant impact on not only flooded alluvial plains and riverine habitats but also on petroleum exploration, production, and transportation activities. Therefore, the implementation of tools to assess the potential impact of oil spills in the Amazonian rivers must be adjusted to the local conditions. The main deliverables of the research are (1) fluvial oil spill sensitivity index maps contemplating each phase of the hydrological cycle (low water, high water, receding water, and rising water), (2) a computational method to represent fluctuations of the seasonal inundation, and (3) a risk analysis method using linguistic rules for the construction of a risk matrix.

Keywords: Amazon region, fluvial sensitivity to oil spills, computational modeling, linguistic rules, risk matrix

1. Introduction

The Amazon is a region characterized by ecologically complex environments subjected to constant and rapid seasonal changes. The environmental patterns that make up the Amazonian scenario are determined by the changes that occur in the different phases of its hydrological cycle. The seasonal dynamic is evidenced by the average annual variation of the waters between maximum drought and flood conditions, which is on the order of 10–12 meters and is associated with rainfall in the headwaters of the rivers of the region and the annual thaw of the Andean summer [1].

A significant quantity of sediments from the Andes slopes, as well as a high concentration of nutrients, is transported during the flood period. This is the

main contributor responsible for the productivity of Amazonian floodplains, in terrestrial and aquatic systems alike [2]. The resulting annual deposition of such sediments defines the fauna and flora, the geomorphology of the floodplain, biogeography, and patterns of human occupation [1].

The discovery and exploitation of oil and gas in the Central Amazon rainforest is a major challenge for sustainable development. Hydrocarbon transportation is an industrial enterprise that involves various potential environmental impacts, thus requiring interdisciplinary studies for risk assessment [3, 4].

The study area includes the flow route of crude oil, liquefied petroleum gas (LPG), and natural gas produced by Petrobras in the Petroleum Province of Urucu. Three pipelines are used to bring crude oil, LPG, and natural gas from Urucu to a terminal located in Coari. From there, crude oil and LPG are transported to Manaus by river, while natural gas is taken via a terrestrial gas pipeline. Thus, this region is susceptible to possible damages due to oil activities, which are a potential threat to environmental conservation in the areas under its influence [5, 6].

The major oil companies have intensified their programs of excellence in environmental management and operational safety in order to reduce the risk of accidents in the operations of exploration, production, and transportation of petroleum and its derivatives. Nevertheless, these accidents can occur in rivers or at sea, due to product spills during procedures of oil tanker reservoir cleaning or loading in terminals, which require standardized response procedures for such emergencies [7].

Thus, given that the Amazon region presents considerable environmental sensitivity to oil spills, there is a need to respond proactively to possible accidents. In order to do this, it was necessary to examine the list of features of its rivers and lakes and their corresponding sensitivity in more detail, in order to hierarchize them in terms of potential impacts [8]. As a result, Araújo et al. [9] defined the fluvial sensitivity index to oil spills, adapted to the corresponding features and consistent with the typical Amazonian seasonality.

Among the factors that influence the sensitivity of habitats to oil spills, the most important are (1) the degree to which affected areas are exposed to processes of natural removal, (2) biological productivity and recovering capability after oil impacts, (3) existing land-use practices, and (4) ease of oil spill cleaning [10]. The overall sensitivity of natural habitats to oil spillage is ranked according to the aforementioned factors in the context of the environmental sensitivity index (ESI). The use of ESI is fundamental for oil spill contingency planning.

The most sensitive habitats in the Amazon region are flooded forests. In fact, inundation causes seasonal differences in the water level and changes the landscape, which creates the need for production of a specific sensitivity index map for each season: low water, high water, receding water, and rising water. The areas occupied by flooded forests change with time, such that continuous monitoring is required through the collection, processing, and analysis of remote sensing data. These areas were first systematically studied in the last decade using LHH SAR images based on the multi-seasonal coverage of the JERS-1 satellite [11].

The global weather-independent coverage provided by the synthetic aperture radar (SAR) system onboard the JERS-1 satellite allowed end users to monitor the rapidly changing conditions in cloud-covered rainforest regions. This L-band, HH polarization system is best suited for flood mapping in rainforest-covered areas due to its capability to penetrate dense vegetation [12].

The JERS-1 satellite orbital arrangement favors the continuous monitoring of the Amazonian hydrological cycle. To do so, contiguous orbits on consecutive days are used. Such a procedure allows temporally homogeneous images to be acquired on a continental scale [13]. Consequently, JERS-1 SAR data were instrumental in mapping inundation variation in space and time over large forested floodplain regions [14–18].

In this chapter, a brief summary will be presented on how the main Amazon features were identified and hierarchized, with relevance to the determination of the environmental sensitivity to oil production and transportation activities. Next, the three approaches used in mapping the fluvial sensitivity index to oil spills, in the stretch that covers Urucu, Coari, and Manaus, will be presented.

2. Determination of the fluvial sensitivity index in the Amazon

Since the beginning of the 1990s, Petrobras has verified that the methodology of drawing up maps of environmental sensitivity to oil spills, adopted by the National Oceanic and Atmospheric Administration (NOAA), adequately adapts to the Brazilian reality, due to its great acceptance and utilization in many countries, as well as the ease of operational implementation [8].

Riverine features of the Amazon region	
Fluvial channel features	**River plain features**
1. River banks (large class subdivided into more precise characteristics) and islands	1. Exposed lake/plain
2. Beaches along the banks	2. Dense flooded forest
3. Waterfalls	3. Bushland (lower-density forest)
4. Riverine sand bars—beaches formed in the middle of the river, isolated from the shores	4. Herb or grass macrophyte bank/exposed plain, depending on the period, functions as a filter
Transitional features between channel and river plain components	
1. Holes	
2. Lake outlets	
Fonte: Petrobras [21].	

Table 1.
Amazon region riverine features.

Index	**Characteristic or feature**
1	Man-made structure
2	Rocky shoals
3	Rapids/waterfalls
4	Scarps/high banks in unconsolidated sediment
5	Exposed beaches and sand/gravel bars
6	Sheltered beaches and sand/gravel bars
7	Exposed mud beaches and bars
8	Sheltered mud beaches and bars
9	River and lake confluence zones
10a	Aquatic macrophyte bars
10b	Scrub-shrub wetlands (swampland, lowland, bushland, field, etc.)
Fonte: Petrobras [21].	

Table 2.
Fluvial sensitivity index to oil spills of the Amazon region.

NOAA's environmental sensitivity classification system is based on the knowledge of geomorphological characteristics of intertidal regions or river and lake limits. In the case of the Amazon basin, because of the need to map the areas under the influence of petroleum production and transportation, it was necessary to hierarchize its ecosystems, after listing its fluvial features. This is necessary because the yearly water level variation results in the flooding of a large portion of the alluvial plain [19, 20]. This area comprises a complex ecosystem composed of lakes, flooded forest, macrophytes, and other habitats (**Table 1**) [21].

Subsequently, taking into account local characteristics of specific features, Araújo et al. [21] defined the different degrees of fluvial sensitivity to oil spills of the Amazon region (10b is the most sensitive; **Table 2**).

3. Study area

The study area embraces the Urucu Petroleum Province; the vicinity of the city of Coari, located near the petroleum terminal (TESOL); the Solimões River stretched up to the Petrobras refinery in Manaus (Reman), in which transportation of crude oil and LPG takes place; and part of the area occupied by the terrestrial gas pipeline (**Figure 1**).

Because it is a region devoid of infrastructure that is subject to a strong seasonal variation of the water level in the river plain, travel between Manaus and the adjacent municipalities is possible only by air or waterway. The main waterways present in the study area include the Tefé, Urucu, Coari, Manacapuru, Purus, and Solimões rivers, in the stretch from Coari to the confluence of the Rio Negro in Manaus (**Figure 1**). Some lakes are present in this region; the most expressive, in account of its size and strategic location, is Lake Coari.

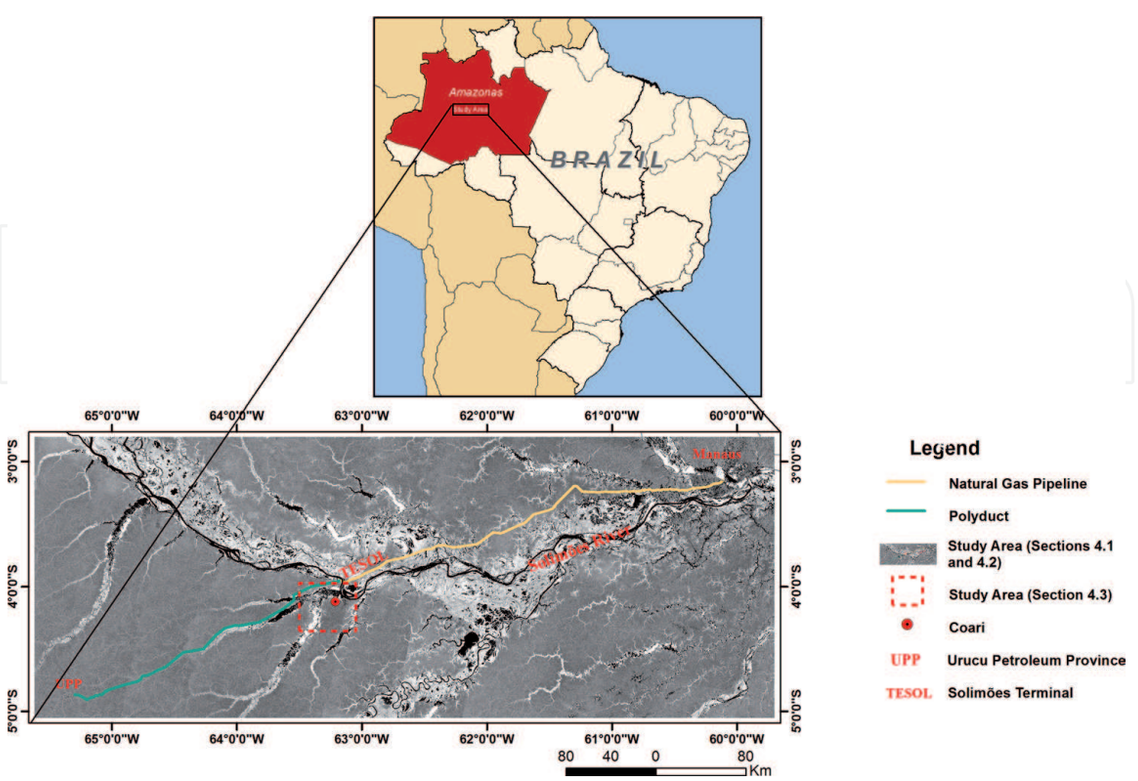

Figure 1.
Study area location on the JERS-1 SAR LHH image msaic (high water). Red rectangle corresponds to ***Figure 8****; red circle is Coari city.*

4. Thematic products

4.1 Fluvial oil spill sensitivity index maps

Environmental sensitivity index maps should reflect the impact of landscape change as a result of flooding. The JERS-1 SAR image mosaics in the low water and high water seasons [22] are input to the unsupervised semivariogram textural classifier (USTC). This algorithm performs image classification, thus recognizing upland forest, flooded forest, flooded vegetation (low biomass above water), and water bodies. A by-product of the classification procedure is the map depicting classes of change, which expresses the difference between dry and flooded seasons.

4.1.1 The USTC classifier

When texture is more important than spectral information, remote sensing image classification must rely on spatial structure. This is the case for the JERS-1 SAR system, which operated using single frequency (L-band) and single polarization (HH). Therefore, the classifier should take into account a pixel in the context of its neighborhood. One possible approach is to analyze texture by means of the semivariogram function [23].

JERS-1 SAR data have already been successfully submitted to semivariogram classification as an aid to vegetation mapping [17, 24]. The unsupervised semivariogram textural classifier (USTC) considers the spatial structure of remote sensing data to carry out image classification. Both textural and radiometric information are combined in this algorithm.

Consider an image dataset X = {x(t) ∈ R,t = 1,...,N}, where each element is a pixel that represents the radiometric information conveyed by the Frost filter digital number (DNdsp) value. Textural information is captured by the semivariogram function γ(t,h) (Eq. (1)):

$$\gamma(t,h) = \frac{1}{2n}\sum_{i=1}^{n}\left(x_h(t,i) - x(t)\right)^2 \tag{1}$$

where x(t) is the pixel value; h is a parameter that controls the extent of the neighborhood, such that the pixels $x_h(t,i)$ lie inside the circle of radius h centered at the pixel x(t); and n is the number of pixels of the neighborhood.

The value $x_h(t,i)$ in (1) is the value of the neighborhood pixel for i = 1...n, in a neighborhood of h defined by the circular semivariogram function γ(t,h) as the texture descriptor. Each pixel in the image is thus transformed into the h + 2 dimensional vector (Eq. (2)):

$$\mathbf{z}(t) = \left[x(t), \gamma(t,1), \gamma(t,2)..., \gamma(t,h), \sigma_h^2(t)\right] \tag{2}$$

where $\sigma_h^2(t)$ is the variance of the area $x_h(t,i), i = 1...n$.

The classification procedure is accomplished based on all components of this h + 2 dimensional vector, calculated for each pixel location. The training set for the unsupervised classification is the set $Z = \{z(t) \in R^{h+2}, t = 1,...,N\}$.

The clustering algorithm known as ISODATA [25] is utilized to perform the unsupervised classification of this set of vectors. At last, clustering results are interactively merged together to define aggregates of one or more classes capable of bearing thematic significance.

4.1.2 Results of UTSC classification

Results of the USTC image classification for the dry (low water) and flooded (high water) seasons are shown, respectively, in **Figures 2** and **3**. Pixels are represented as follows: upland forest in green, water bodies in blue, flooded forest in yellow, and flooded vegetation in light blue.

After definition of the dual season USTC-classified products, a post-classification change detection algebraic calculation generated a multi-temporal landscape change map, corresponding to half hydrological cycle in the Central Amazon region (i.e., from dry to flooded seasons).

The landscape change map depicted in **Figure 4** represents all possible combinations of classes detected using the USTC method. Some of them are rare or would seem impossible to occur in the transition from dry to flooded seasons, such as C15 (flooded forest/upland forest), while others describe most of the pixels such as C16 (upland forest/upland forest). Some classes such as C12 (upland forest/flooded forest) should be highlighted because they indicate increased environmental sensitivity to oil spills from low water to high water in river plains. This map is an important input for generation of a temporal environmental sensitivity index. In this study, such a product refers to the transition from low water in September 1995 to high water in May 1996, when orbital images were obtained for JERS-1 SAR mosaic composition.

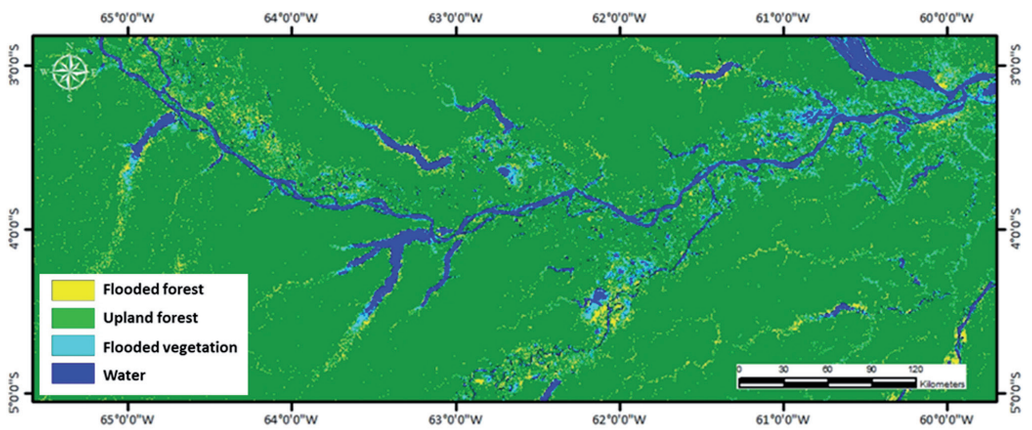

Figure 2.
USTC result for the dry season (October 1995; low water). Modified from [11].

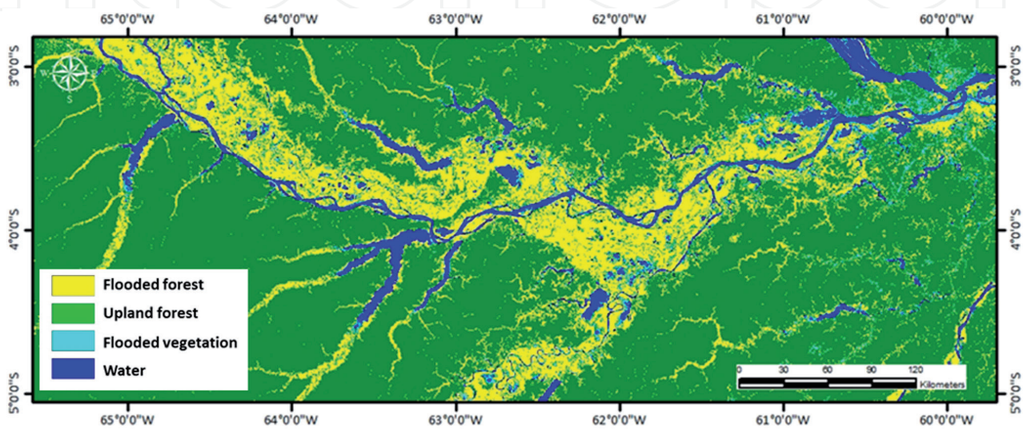

Figure 3.
USTC result for the flooded season (may 1996; high water). Modified from [11].

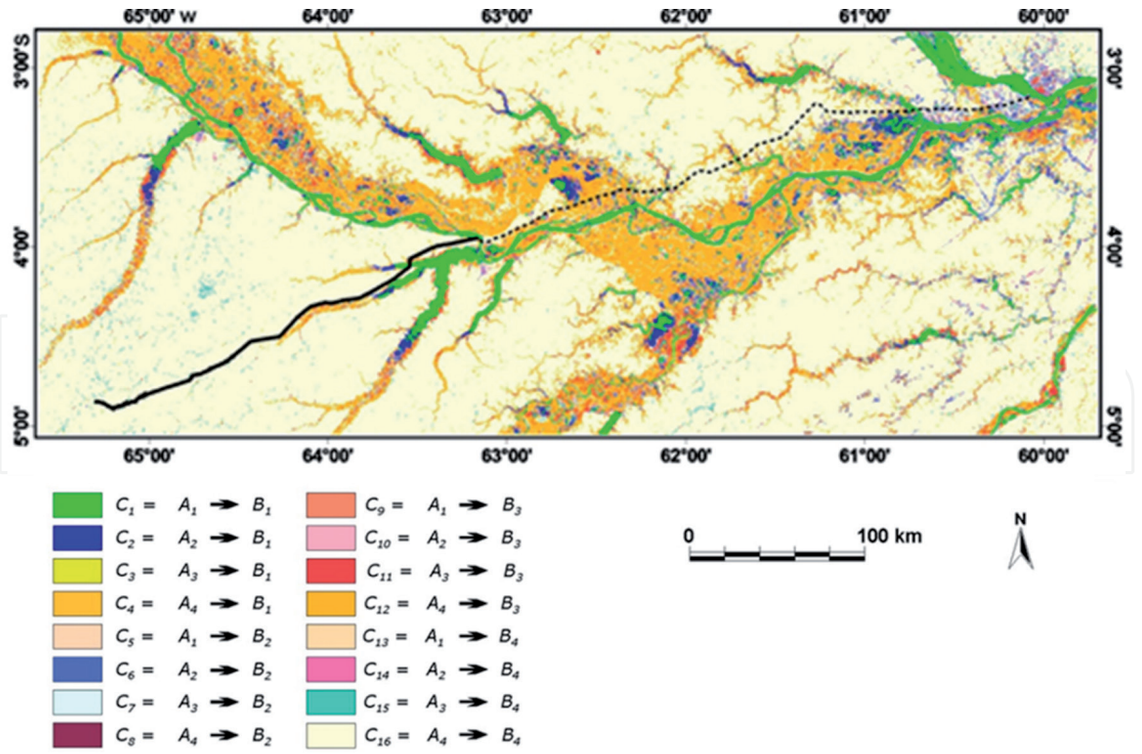

Figure 4.
*Landscape change map from October 1995 (low water) to May 1996 (high water). Modified from [11] (see **Table 3** for the definition of classes of change (C1 to C16).*

4.2 An analytical method using linguistic rules for the construction of a risk matrix

4.2.1 The risk matrix

One way to qualitatively or semi-quantitatively assess risk is to create a ranking with a risk matrix [3, 26]. According to Markowski and Mannan [27], a risk matrix (RM) is a tool that subjectively allows for the assessment of different analytical processes. The basis for defining a RM is the association of severity or possible consequences in each scenario with the frequency with which certain event occurs. A RM is developed through the following steps: (1) characterization and scaling of the severity of the consequences and the frequency of an event, (2) characterization and ranking of the risk, (3) establishment of the basic rules focused on the risk, and (4) graphical editing of the risk matrix.

Risk matrix		**Probability of hydrological change**				
		Extremely unlikely	**Unlikely**	**Rare**	**Likely**	**Frequent**
Environmental sensitivity to oil spill	Catastrophic	0.20	0.40	0.60	0.80	1.00
	Critic	0.15	0.30	0.45	0.60	0.75
	Marginal	0.10	0.20	0.30	0.40	0.50
	Negligible	0.05	0.10	0.15	0.20	0.25

Table 3.
The risk matrix for the impact of an oil spill in Amazonian environments subject to changes due to flooding.

The number of hierarchical levels should be determined as needed by the problem. Considering the environmental sensitivity to oil spills, they may, for example, be designated as catastrophic, critical, marginal, and negligible. The graphical representation of the risk matrix should be simple in order to easily convey the risks involved in a set of rules.

A RM was developed to assess the environmental risk for oil spills in the Amazonian landscape within half hydrological cycle based on the following predefined rules: (1) landscape changes that exist are reliable within half hydrological cycle (from drought to flood), and (2) the environmental impacts of an oil spill depend on variations of the hydrological regime. The combination of these two sets of rules can provide the environmental risk involved in oil pipeline and fluvial transportation for each combination of landscape change (**Tables 3** and **4**).

4.2.2 Fuzzy modeling of the environmental sensitivity

The use of fuzzy logic allows for the capture and integration of scientific and local expert knowledge about the phenomenon being studied using heuristic "if-then" rules [26]. Fuzzy logic provides a powerful approach for classifying and monitoring environmental conditions related to flooding and describing the nature and severity of changes occurring over time.

The fuzzy modeling employs a symbolic representation of those classes, which is used to estimate the risk of each type of landscape change, based on the linguistic interpretation of the symbols and the RM defined in Section 4.2.1. The fuzzy modeling computes the function that converts the classes of change into levels of risk, as defined by the rule set in Eq. (3). In the present study, n = 16 classes of change will be mapped into m = 3 classes of risk. The fuzzy model is conveniently computed as a TS model (Eq. (4)), where risk is represented by a continuous parameter vector

Class of change	Class name: dry season	Class name: flooded season	Level of risk	θ
C1	Water	Water	Low	**0.25**
C2	Flooded veget.	Water	Intermediate	**0.4**
C3	Flooded forest	Water	Intermediate	**0.4**
C4	Upland forest	Water	Low	**0.3**
C5	Water	Flooded veget.	Low	**0.3**
C6	Flooded veget.	Flooded veget.	High	**1**
C7	Flooded forest	Flooded veget.	High	**0.8**
C8	Upland forest	Flooded veget.	Intermediate	**0.6**
C9	Water	Flooded forest	Low	**0.3**
C10	Flooded veget.	Flooded forest	Intermediate	**0.4**
C11	Flooded forest	Flooded forest	High	**1**
C12	Upland forest	Flooded forest	Intermediate	**0.6**
C13	Water	Dry forest	Low	**0.1**
C14	Flooded veget.	Dry forest	Low	**0.1**
C15	Flooded forest	Dry forest	Low	**0.1**
C16	Dry forest	Dry forest	Low	**0.25**

Table 4.
Level of risk for each class of change and the respective model parameters.

$\theta \in R^n$, in which each component represents the environmental sensitivity index of each class of landscape change:

$$u_k(t) = \frac{\|\mathbf{x}(t) - \boldsymbol{\omega}_k\|^{\frac{2}{\gamma-1}}}{\sum_{k=1}^{n}\|\mathbf{x}(t) - \boldsymbol{\omega}_k\|^{\frac{2}{\gamma-1}}}, \quad (3)$$

where $\varpi_k \in R^2$ is the coordinates of the center of each class of change k, $k = 1, \ldots n$, and γ is the parameter that adjusts the fuzziness of the membership function, i.e., the grade that membership functions overlap, usually $1.2 \leq \gamma \leq 2.0$:

$$C_k \rightarrow L_l, \; k = 1, \ldots n \;\; l = 1, \ldots, m \quad (4)$$

The temporal environmental index is computed from the input variable defined in R^2, which represents the backscatter space of the dry and flooded season data, following the work of Hess et al. [28]. The input variable is the vector x(t) = [x_D (t), x_F (t)], where x_D (t) is the coefficient of backscatter LHH in the dry season (dB) and x_F (t) is the coefficient of backscatter LHH in the flooded season (dB).

The fuzzy model computes a smooth approximation of the risk values of each class of change according to the membership vector of each pixel to the classes of change.

4.2.3 The temporal environmental sensitivity index map

The map depicting temporal environmental sensitivity index (TESI) values is presented in **Figure 5**. They range in the interval [0,1] in order to avoid abrupt transitions between contiguous landscape change classes. The achieved results portray a broad spectrum of flooded forest with TESI values between 0.6 and 0.7, as well as several minor regions with higher values.

The TESI values obtained by the proposed methodology were compared with field checks at the Coari terminal (TESOL). **Figure 6** presents the map of the 16 landscape change classes and the TESI map. Inserted in each panel of **Figure 6** are the location of each field checkpoint and profiles of different values of the TESI obtained by the fuzzy modeling approach.

At PT06, people live on the bank of the river, occupying a small space on stilts surrounded by different flooded and dried plant species (**Figure 13h**). The landscape change map assigns PT06 to class C4, which corresponds to upland forest that

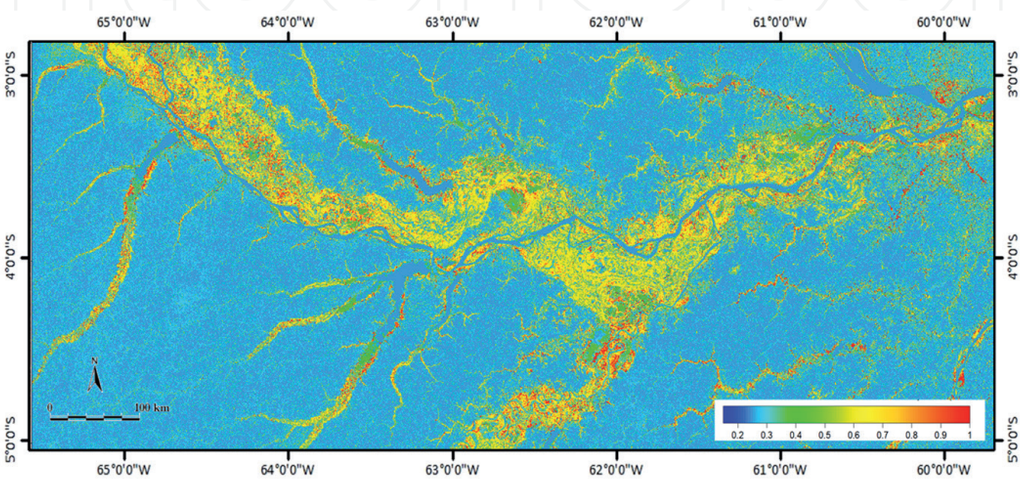

Figure 5.
Results of the temporal environmental sensitivity index (TESI).

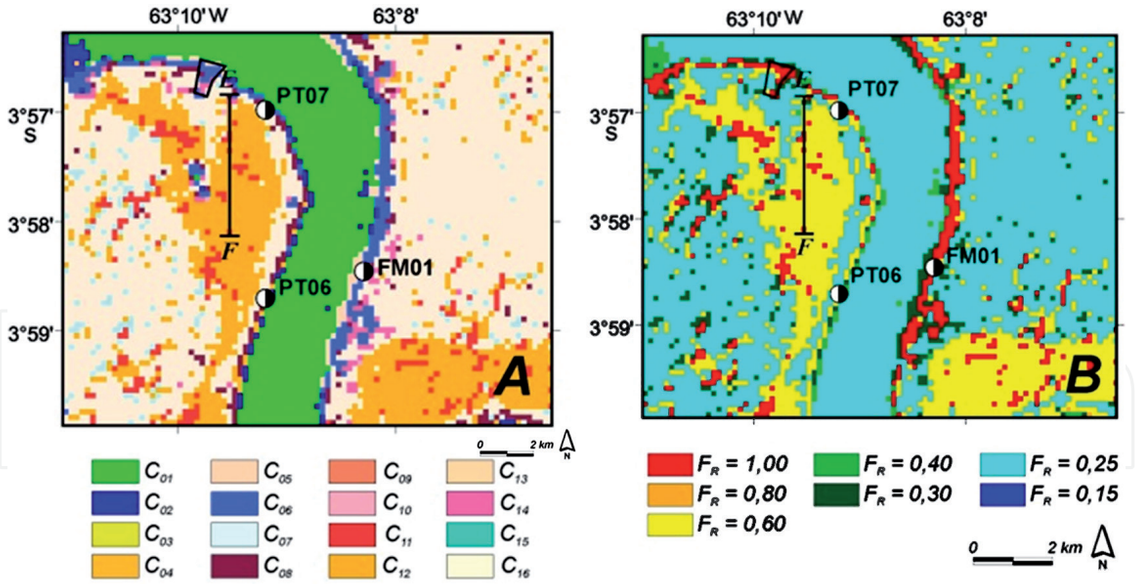

Figure 6.
Area in the vicinities of Coari, with field checkpoint location. (A) Landscape change map; (B) the map of TESI.

is covered by water (i.e., completely drowned) in the flood season. For this point, TESI = 0.5810; the local environmental conditions suggest that this value agrees well with the intermediate risk assigned to this area.

In PT07, near TESOL (**Figure 13g**), it is possible to clearly see the closed canopy of the flooded forest, with only the tree tops and a few trunks above the waterline. The C8 class indicates that the upland forest is flooded here in the high water season. The TESI value shows that PT07 has an intermediate risk if oil is spilled there.

4.3 A computational method to represent fluctuations of the seasonal inundation

The following data were used in this part of the study:

- JERS-1 SAR mosaics submitted to the USTC classification procedure.
- SRTM C-band data, located in the border portion of Sheet SB.20-V-B, as a basis for the extraction of altimetric information.
- SWBD mask (SRTM Water Body Data), which is a by-product of the digital elevation model (DEM) generated by SRTM, with the objective of portraying bodies of water that meet the minimum criteria of capture, which resulted in the identification and delimitation of lakes and rivers existing in the region of Coari, in the shapefile vector format.
- Data of fluviometric measurements acquired through the National Water Agency (ANA), where a historical series of water level in Coari was obtained, from 1982 to 2010, which made it possible to infer the main moments of the water regime of the area investigated, characterized by low water, high water, receding water, and rising water.

It is worth mentioning that under the dense vegetation conditions of the Amazonian environment, there are limitations of the SRTM altimetry, which refer to the crown of the trees in the C bands. Therefore, it is necessary to this DEM with other sources of information, in order to produce a proper interpretation.

Using SRTM data, it was possible to develop the following cartographic products:

- **Topographic contour lines**, which show the low altitudinal amplitude characteristic of the region, as a very unfavorable condition to the analysis, aggravated by the SRTM DEM ambiguity, as mentioned above. This reflects the limited penetration in the canopy of the radar pulse, because the Amazonian biome is predominantly composed of dense forest (trees with an average height of 20 meters). Therefore, it is necessary to interpret the contour lines together with the USTC-classified JERS-1 SAR mosaics. Such a procedure allowed verifying that the limits of potentially floodable areas coincide with the 40 m contour line. Furthermore, in the terrain located below this topographic level, there are flooded forests and macrophyte banks. It was also verified, locally, that the greater penetration in the vegetation of the JERS-1 SAR L-band signal allowed the delineation of flooded forests even above 40 meters (**Figure 7**). The criterion used to consider the terrain below 40 m as constituted by flooded forests and macrophyte banks, when the maximum water level in Coari occurs (approximately 20 m) and also taking into account the average tree height in the Amazon region (20 m). According to the fluvial sensitivity index to oil spills [5], the aforementioned areas, during the flood season, correspond to 10b (flooded vegetation) and 10a (aquatic macrophytes) (**Table 2**).

- **The elevation map** (**Figure 8**), showing the altimetric classes derived from the contour lines, allows to point out features that are not very prominent in the landscape, but which configure steep stretches along the shores of Coari and Mamiá lakes. An expressive drainage network was developed in the most elevated areas, which are not, however, subject to flooding. On the other hand, the removal of the vegetation cover allows the hydrographic network to be exposed more clearly in the periphery of the urban center of Coari. The distribution of the altimetric classes reveals the presence of characteristic features of the investigated area, such as plateaus and floodplains with many depressions [6].

- **The slope map** (**Figure 9**), in which flat relief corresponds to slopes varying from 0 to 3.7%, gentle undulations range from 3.7 to 9.3%, and moderate undulations whose present slopes above 10%. In this product, significant terrain features are observed, such as the plateaus (cyan) that are not restricted to a single hypsometric unit, since they occur in different altitudes. In addition, there are very steep river banks, which are naturally more susceptible to erosion.

In addition to the cartographic products, the water-level historical series of Coari was examined (**Figure 10**). This permitted to infer the different phases of the hydrological cycle. Thus, in the flood period, rivers can reach up to approximately 18 meters, while in the most intense droughts, the water can reach values less than 2 meters. The lowest water level was recorded in October 1998, reaching 1.86 m; the largest flood occurred in July 1999 with the water level at 17.68 m.

Considering that the acquisition of orbital data for the SRTM mission took place between February 10 and 20, 2000, the analysis of the historical series also made it possible to gauge the apportionments in that period for the water level in Coari, between 932 and 985 centimeters.

The water level during the SRTM mission (February/2000) ranged between 932 and 985 cm.

After performing the procedures mentioned above, it was necessary to implement algorithms on MatLab to use a morphological operator, known as watershed,

described by Meyer [29] and with an algorithm elaborated by Gonzalez [30]. The objective was to simulate a flood process on the hypsometric map extracted from SRM DEM. This technique interprets the gray-scale image as the expression of the

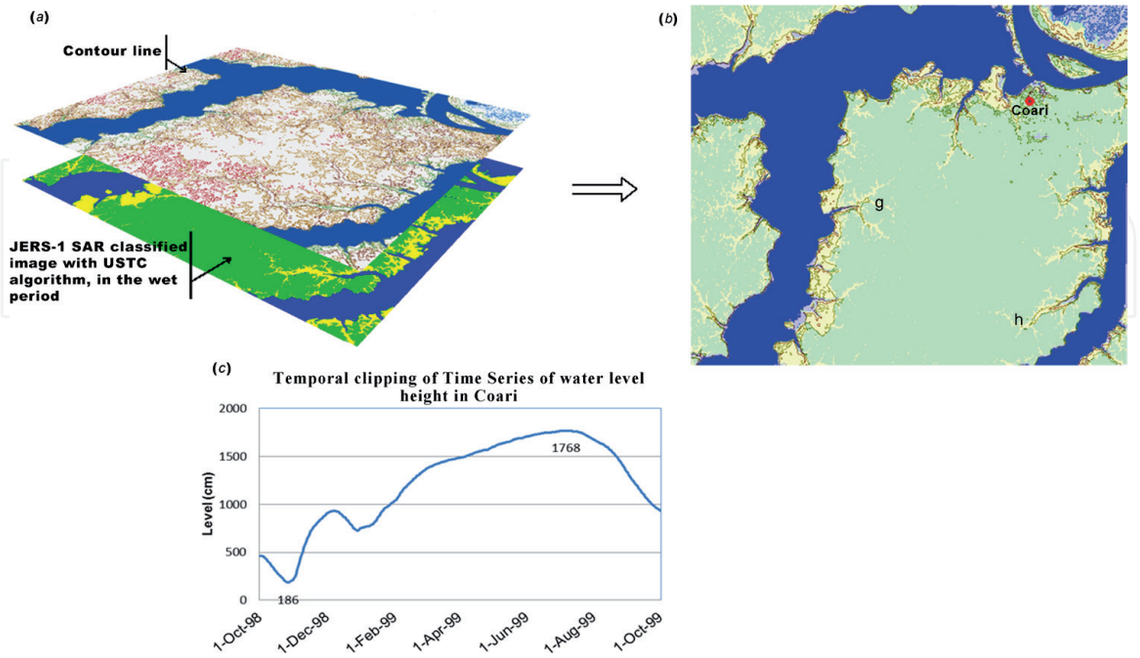

Figure 7.
Illustrative diagram using 40-m contour lines, superimposed on the USTC-classified JERS-1 SAR mosaic at the high-water period (a), resulting in the interpretation of (b). The inserted time series shown in (c) indicates the maximum and minimum water levels in the Coari region. The areas in yellow represent flooded forests in USTC classification of JERS-1 SAR images. Letters (g) and (h) refer to flooded forest stretches in areas higher than the 40-m level, with restricted spatial distribution. Source: Silva et al. [6].

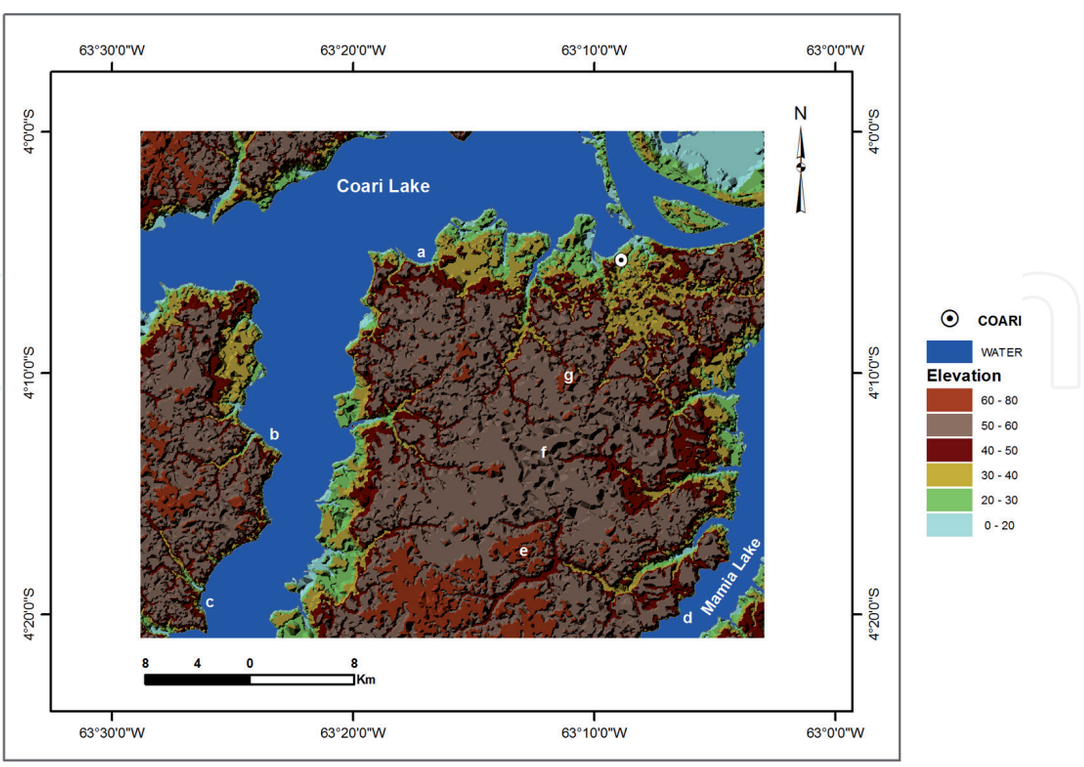

Figure 8.
*Elevation or hypsometric map of Coari with altimetric classes ranging from 0 to 80 m (see **Figure 1** for location). Compare with the location of flooded forest areas in Figure 8. In a, b, c, and d, there are examples of steep scarps on the margins of the Coari and Mamia lakes. In e, f, and g, the relief seems to be structurally controlled by geologic features oriented roughly E-W. Source: Silva et al. [6].*

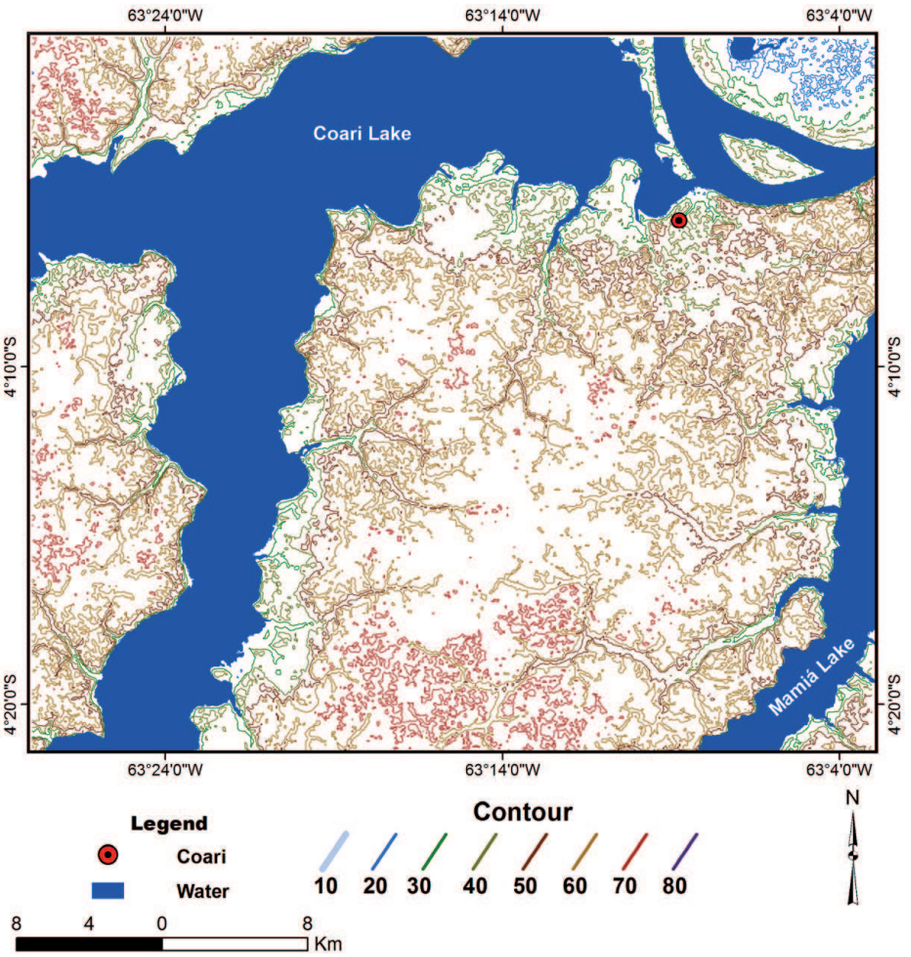

Figure 9.
Slope map, in which the gradient is calculated as a percentage. Source: Silva et al. [6].

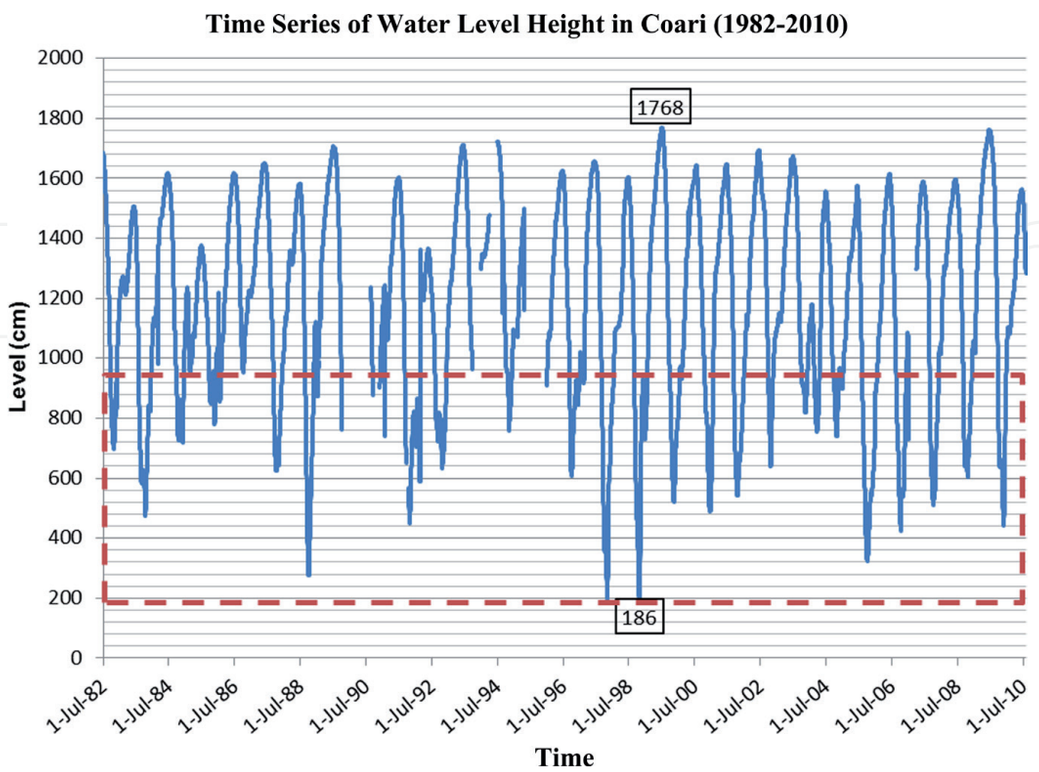

Figure 10.
Water-level time series in Coari, indicating the maximum high- and low-water periods, as well as the levels below observations carried out in the SRTM data acquisition period (red rectangle). Source: Silva et al. [6].

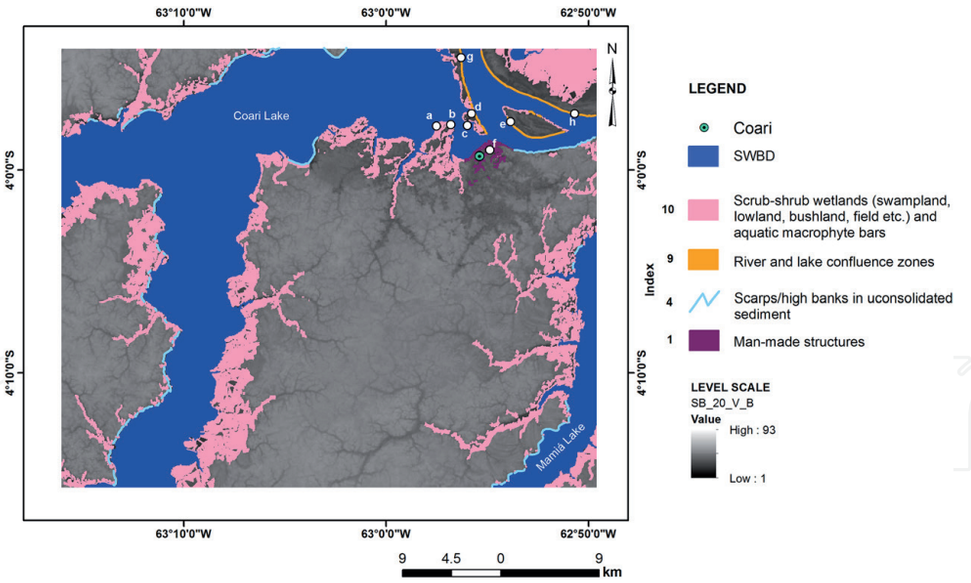

Figure 11.
*Fluvial oil spill sensitivity index map in the Coari region (AM) during the high-water period, according to the criteria established in Araújo et al. [9] and as a modification of Petrobras [21]. Stretches from the slope map (**Figure 9**) corresponding to steep scarps are assigned to index 4. The points a, b, c, d, e, f, g, and h can be seen in **Figures 12** and **13**. Index 10 shown here includes 10a and 10b from **Table 2**.*

Figure 12.
*Photographic records of points checked in the field (27 May 1998; high-water period) in Lake Coari, where it is possible to observe (a) flooded forest, (b) aquatic macrophytes, (c) flooded forest, (d) aquatic macrophytes, (e) Ariá Island, Solimões River, and (f) aerial photograph of Coari city at the confluence of Lake Coari and Solimões River (see **Figure 11** for location). Source: Silva et al. [6].*

Figure 13.
Photographic records of points checked in the field, where it is possible to observe (g) panoramic view obtained in August 2008, upstream of the Solimões River's confluence with Lake Coari. From this point downstream, inundation in the high-water period contributes to the formation of the Ariá Island, (h) right margin of the Solimões River exhibiting evidence of erosion (see ***Figure 11*** *for location). Source: Silva et al. [6].*

topographic relief, where at each level an altitude is assigned proportional to its value, so that the procedure "flood the image" from the lower regions gradually submerges the features. By simulating the flooding process, the watershed morphological operator works with the water level information to make the results reliable. In fact, the flooding process starts from the maximum water level value found in the SRTM mission period (985 cm).

This method carried out a classification that maps areas of the same topographic meaning in the image. In this procedure each pixel was incorporated into a cluster by the measure of similarity of Euclidean distances. The classifier compares the Euclidean pixel distance to the average of each cluster, iteratively, until the entire image is sorted. Thus, for each level, segments were obtained by configuring the flood limits, duly obeying the topographic levels, as per the maximum value, in which the highest level of fluvial apportionment in Coari was recorded, and the minimum value, referring to the SRTM mission date which corresponds to the flood period of the Amazonian hydrological cycle (February 2000).

Figure 11 shows the results achieved with this approach, which successfully integrated the products discussed so far, i.e., the criteria for fluvial environmental sensitivity to oil spills in the Amazon region, the cartographic products extracted from the SRTM DEM, and the Coari water-level time series.

It is possible to verify in **Figure 11** the predominance of index 10 inside the Coari and Mamiá lakes (considering the fusion of classes 10a and 10b of **Table 2**). In these lakes, the segments of its banks are attributed to index 4 and are associated with escarpments developed in the sedimentary cover in the presence of corrugated relief subject to erosion by the fluvial action (**Figure 11**). Similar escarpments are observed on the right bank of the Solimões River, downstream of the city of Coari. Other sites in **Figure 11** were classified as confluent zones of rivers and lakes (index 9), as shown in **Figures 12e, 13g** and **h**. **Figure 8e** shows a strip of land on the edge of Ariá Island, located in the Solimões River.

5. Conclusions

The studies herein presented summarize innovative approaches in the use of spaceborne LHH SAR images such as the ones acquired by the JERS-1 SAR satellite, aiming for the development of an environmental sensitivity index to oil spills adequate for the fluvial variations of Central Amazonia, with an initial application for half of the hydrologic cycle. The JERS-1 SAR mosaics correspond to the low water season (September–October 1995) and the subsequent high water season (May–June 1996).

The USTC algorithm enabled the construction of thematic maps to meet the computational requirements of engineering applications that demand the expeditious identification of flooded area maps. In this work, four classes of interest were considered: water, flooded vegetation, upland forest, and flooded forest.

The risk analysis method using linguistic if-then rules derived from expert knowledge and data statistics proved to be an efficient method for remapping 16 landscape change classes. Consequently, this approach could illustrate the potential risks in the fluvial transportation of oil in environments subject to intense seasonal variations in the water level, such as in the Central Amazon.

The procedure based on symbolic fuzzy modeling performed as expected is that it identified the boundaries of landscape change classes using TESI values. Such an approach considered the radiometric centers pertaining to the 16 landscape change classes defined by backscatter values of dry and flooded JERS-1 SAR mosaics.

Finally, the watershed technique satisfactorily represented the seasonality of the flooding process in the study area, as an aid to the determination of the fluvial sensitivity to oil spills in the Coari region. The achieved results offer a new perspective for the elaboration of products using the SRTM DEM in conjunction with the mathematical morphology and the study of water-level time series in the Amazon region.

Acknowledgements

The authors thank the Brazil's National Agency of Petroleum, Natural Gas and Biofuels (ANP), National Council for Scientific and Technological Development (CNPq), Alberto Luiz Coimbra Institute for Graduate Studies and Research in Engineering (COPPE), and Federal University of Rio de Janeiro (UFRJ) for their support in the development of this research.

DOI: http://dx.doi.org/10.5772/intechopen.86592

Author details

Patricia Mamede da Silva[1*], Fernando Pellon de Miranda[1], Carlos Henrique Beisl[1], Luiz Landau [1] and Alexandre Gonçalves Evsukoff [1,2]

1 Laboratory for Computational Methods in Engineering (LAMCE), Federal University of Rio de Janeiro (UFRJ), Rio de Janeiro, Brazil

2 Technology Transfer Nucleus (NTT), Federal University of Rio de Janeiro (UFRJ), Rio de Janeiro, Brazil

*Address all correspondence to: patmamed@lamce.coppe.ufrj.br

References

[1] Queiroz HL. A reserva de desenvolvimento sustentado Mamirauá: Um modelo de alternativa viável para proteção e conservação da biodiversidade na Amazônia. Dossiê Amazônia II—Revista de Estudos Avançados—IEA/USP. 2005;**19**(54):183-203

[2] Richey JE, Meade RH, Salati E, Devol AH, Nordin CF Jr, et al. Water discharge and suspended sediment in the Amazon River: A sampling procedure and distributions. Water Resources Research. 1986;**22**:756-764

[3] Tena-Chollet F, Tixier J, Dusserre G, Mangin J-F. Development of a spatial risk assessment tool for the transportation of hydrocarbons: Methodology and implementation in a geographical information system. Environmental Modelling & Software. 2013;**46**:61-74

[4] Sowmya K, Jayappa K.S. Environmental sensitivity mapping of the coast of Karnataka, west coast of India. Ocean and Coastal Management. 2016;**121**:70-87

[5] Jensen JR, Narumalani S, Weatherbee O, Murday M, Sexton WJ, et al. Coastal environment sensitivity mapping for oil spills in the United Arab Emirates using remote sensing and GIS technology. Geocarto International. 1993;**2**:5-13

[6] Silva PM, Miranda FP, Landau L. Mapping the Brazilian Amazon Fluvial Sensitivity Index to Oil Spills with Shuttle Radar Topography Mission (SRTM) Data. Geocarto International. 2018;**33**(6):555-572

[7] Petersen et al. NOAA Environmental Sensitivity Index Guidelines Version 3.0. NOAA Technical Memorandum NOS OR&R 11. 2002

[8] PETROBRAS. Mapas de Sensibilidade Ambiental a Derrames de Óleo—Ambientes Costeiros, Estuarinos e Fluviais. Rio de Janeiro: Editora Jauá; 2006. p. 166

[9] Araújo SI, Silva GH, Muehe DCEH. Manual Básico para Elaboração de Mapas de Sensibilidade Ambiental a Derrames de Óleo no Sistema Petrobras: Ambientes Costeiros e Estuarinos. Rio de Janeiro: Petrobras; 2002. p. 133

[10] National Oceanic and Atmospheric Administration (NOAA) and American Petroleum Institute (API). Inland Oil Spills: Options for Minimizing Environmental Impacts of Freshwater Spill Response. American Petroleum Institute Publ. No. 4558. Seattle and Washington, D.C.: NOAA and API; 1994. p. 130

[11] Beisl CH, Miranda FP, Evsukoff AG, Pedroso EC. Assessment of environmental sensitivity index of flooding areas in Central Amazon using fuzzy logic in the dual season GRFM JERS-1 SAR images mosaics. In: Proceedings of IGARSS, Toulouse, França; 2003

[12] Schmullius CC, Evans DL. Synthetic aperture radar (SAR) frequency and polarization requirements for applications in ecology, geology, hydrology, and oceanography: A tabular status quo after SIR-C/X-SAR. International Journal of Remote Sensing. 1997;**18**:2713-2722

[13] Rosenqvist A, Shimada M, Chapman B, Freeman A, De Grandi G, Saatchi S, et al. The global rain forest mapping project—A review. International Journal of Remote Sensing. 2010;**21**(6-7):1375-1387

[14] Costa MPF, Novo EMLM, Ahern F, Pietsh RW. Seasonal dynamics of the Amazon floodplain through RADAR

eyes: Lago Grande de Monte Alegre case study. In: Proceedings of the International Symposium Geomatics in the Era of RADARSAT (GER'97); 1997. paper available in CD-ROM format

[15] Freeman A, Chapman B, Siqueira P, Hess L, Holt J, Dutra L. Mapping Inundation of the Amazon Basin. JERS-1 Science Program '99 PI Reports: Global Rainforest Monitoring and SAR Interferometry; 1999. pp. 49-54

[16] Hess LL, Melack JM, Simonett DS. Radar detection of flooding beneath the forest canopy: A review. International Journal of Remote Sensing. 1990;**11**(7):1313-1325

[17] Miranda FP, Carr JR. Application of the semivariogram textural classifier (STC) for vegetation discrimination using SIR-B data of the Guiana shield, Northwestern Brazil. Remote Sensing Reviews. 1994;**10**:155-168

[18] Rosenqvist A. Analysis of the backscatter characteristics of rubber, oil palm and irrigated rice in multi-band polarimetric synthetic aperture radar imagery [thesis]. Institute of Industrial Science, University of Tokyo; 1997

[19] Sioli H. Hydrochemistry and geology in the Brazilian Amazon region. Amazoniana. 1984;**1**:74-83

[20] Junk WJ. General aspects of foodplain ecology with special reference to Amazonian foodplains. In: The Central Amazonian Foodplain: Ecology of a Pulsing System. Berlin: Springer-Verlag; 1997

[21] Araújo SI, Silva GH, Muehe DCEH, Pereira TAA. Adaptação do índice de sensibilidade ambiental a derramamentos de óleo da national oceanic and atmospheric administration—NOAA às feições fluviais Amazônicas. In: Comunicação Técnica BIO No 24. Rio de Janeiro: Petrobras; 2002. p. 40

[22] Chapman B, Siqueira P, Freeman A. The JERS-1 SAR Amazon multi-season mapping study (JAMMS): Observation strategies and data characteristics. International Journal of Remote Sensing. 2002;**23**(7):1427-1446

[23] Carr JR. Spectral and textural classification of single and multiple band digital images. Computers & Geosciences. 1996;**22**:849-866

[24] Miranda FP, Fonseca LEN, Carr JR, Taranik JV. Analysis of JERS-1 (Fuyo-1) SAR data for vegetation discrimination in northwestern Brazil using the semivariogram textural classifier (STC). International Journal of Remote Sensing. 1996;**17**:3523-3529

[25] Ball G, Hall ED. ISODATA, a novel method of data analysis and pattern classification. In: Technical Report NTIS AD 699616. Stanford, CA: Stanford Research Institute; 1965

[26] Sarkar S, Parihar SM, Dutta A. Fuzzy risk assessment modelling of East Kolkata wetland area: A remote sensing and GIS based approach. Environmental Modelling & Software. 2016;**75**:105-118

[27] Markowski AS, Mannan MS. Fuzzy risk matrix. Journal of Hazardous Materials. 2008;**159**(1):152-157

[28] Hess LL, Melack JM, Novo EMLM, Barbosa CCF, Gastil M. Dual season mapping of wetland inundation and vegetation for the Central Amazon Basin. Remote Sensing of Environment. 2003;**87**:404-428

[29] Meyer F. Topographic distance and watershed lines. Signal Processing. 1994;**38**:113-125

[30] Gonzalez RC, Woods RE, Eddins SL. Digital Image Processing using Matlab. Upper Saddle River, New Jersey: Pearson-Prentice-Hall; 2004. p. 620